CHEMISTRY
A EUROPEAN JOURNAL

DOI: 10.1002/chem.200801450

A Novel Ni_4 Complex Exhibiting Microsecond Quantum Tunneling of the Magnetization

Guillem Aromí,*[a] Elisabeth Bouwman,[b] Enrique Burzurí,[c] Chiara Carbonera,[c] J. Krzystek,[d] Fernando Luis,[c] Christoph Schlegel,[e] Joris van Slageren,*[e, f] Stefania Tanase,[b] and Simon J. Teat[g, h]

Dedicated to Professor Jan Reedijk on the occasion of his 65th birthday

Abstract: A highly asymmetric Ni^{II} cluster $[Ni_4(OH)(OMe)_3(Hphpz)_4(MeOH)_3](MeOH)$ (**1**) (H_2phpz = 3-methyl-5-(2-hydroxyphenyl)pyrazole) has been prepared and its structure determined by means of single-crystal X-ray diffraction by using synchrotron radiation. Variable-temperature bulk-magnetization measurements show that the complex exhibits intramolecular-ferromagnetic interactions leading to a spin ground state $S=4$ with close-lying excited states. Magnetization and high-frequency EPR measurements suggest the presence of sizable Ising-type magnetic anisotropy, with zero-field splitting parameters $D=-0.263\ cm^{-1}$ and $E=0.04\ cm^{-1}$ for the spin ground state, and an isotropic g value of 2.25. The presence of both axial and transverse anisotropy was confirmed through low-temperature specific heat determinations down to 300 mK, but no slow relaxation of the magnetization was observed by AC measurements down to 1.8 K. Interestingly, AC susceptibility measurements down to temperatures as low as 23 mK showed no indication of slow relaxation of the magnetization in **1**. Thus, despite the presence of an anisotropy barrier ($U\approx 4.21\ cm^{-1}$ for the purely axial limit), the magnetization relaxation remains extremely fast down to the lowest temperatures. The estimated quantum tunneling rate, $\Gamma > 0.667$ MHz, makes this complex a prime candidate for observation of coherent tunneling of the magnetization.

Keywords: cluster compounds · magnetic properties · nickel · quantum tunneling · relaxation

Introduction

The discovery of stable magnetization at low temperatures in certain molecular clusters sparked an expansion in the field of molecular nanomagnetism in the early 1990s.[1,2] These molecules, known as molecular nanomagnets or single-molecule magnets, consist of a number (typically between 4 and 20) of paramagnetic transition metal ions,

[a] Dr. G. Aromí
Departament de Química Inorgànica, Facultat de Química
Universitat de Barcelona, Diagonal 647, 08028 Barcelona (Spain)
Fax: (+34)934-907-725
E-mail: guillem.aromi@qi.ub.es

[b] Dr. E. Bouwman, Dr. S. Tanase
Coordination and Bioinorganic Chemistry
Leiden Institute of Chemistry, Gorlaeus Laboratories
P.O. Box 9502, 2300 RA Leiden (The Netherlands)

[c] E. Burzurí, Dr. C. Carbonera, Dr. F. Luis
Instituto de Ciencia de Materiales de Aragón
CSIC-Universidad de Zaragoza, y Departamento de
Física de la Materia Condensada
C/Pedro Cerbuna 12, 50009-Zaragoza, (Spain)

[d] Dr. J. Krzystek
National High Magnetic Field Laboratory, Florida State University
Tallahassee, Florida 32310 (USA)

[e] C. Schlegel, Dr. J. van Slageren
1. Physikalisches Institut, Universität Stuttgart
Pfaffenwaldring 57, 70550 Stuttgart (Germany)
E-mail: Joris.Van.Slageren@nottingham.ac.uk

[f] Dr. J. van Slageren
School of Chemistry, University of Nottingham
University Park, Nottingham NG7 2RD (UK)
Fax: (+44) 115-951-3563

[g] Dr. S. J. Teat
Daresbury Laboratory, Daresbury, Warrington
Cheshire WA4 4AD (UK)

[h] Dr. S. J. Teat
Light Source, Lawrence Berkeley Lab
1 Cyclotron Rd, MS2–400, Berkeley, CA 94720 (USA)

Supporting Information (structural parameters of **1** and symmetry groups of $[Ni_4O_4]$ complexes) for this article is available on the WWW under http://dx.doi.org/10.1002/chem.200801450.

which are bridged by simple ligands and surrounded by an organic ligand shell. The small size of these molecules, combined with their absolute monodispersity, makes them potential successors to the magnetic nanoparticles used currently for magnetic data storage. Many fascinating quantum properties were observed in these systems, such as quantum tunneling of the magnetization (QTM),[3,4] quantum phase interference,[5] and quantum magnetic oscillations.[6]

The past intensive research, however, has shown that the requirements for successful application of molecular nanomagnets are quite stringent. The ions in the cluster need to be coupled by the superexchange interaction so that the cluster ground state has a large spin S. Furthermore, the anisotropy of this spin ground state needs to be such that the microstates with the largest magnetic moment ($M_S = \pm S$) are lowest in energy. This anisotropy, characterized by the axial zero-field splitting (ZFS) parameter D and higher-order parameters, creates an energy barrier for inversion of the magnetic moment and hence stable magnetization at low temperatures, with a barrier height given by $U \approx DS^2$ (or $U \approx D(S^{2-} - {}^1/_4)$ if S is half-integer). The spin Hamiltonian which defines the energy levels of the ground state is given by Equation (1), in which the first term is the second-order axial ZFS, and the second is the second-order transverse anisotropy.

$$\mathscr{H}^{\mathrm{ZFS}} = D[\hat{S}_z{}^2 - {}^1/_3 S(S+1)] + E(\hat{S}_x{}^2 - \hat{S}_y{}^2) \quad (1)$$

Transverse ZFS changes the character of the eigenstates of the system from pure M_S states (denoted by $|M_S>$) to symmetric and antisymmetric superpositions of the $\pm M_S$ states, denoted by $|M_S> + |-M_S>$, and $|M_S> - |-M_S>$, respectively, in which normalization constants have been omitted. These states are split by an amount known as the tunnel frequency, and in a time-dependent picture the magnetic moment will oscillate from up to down and back at that frequency. This phenomenon has been named quantum tunneling of the magnetization.[3,4] The process is usually incoherent: that is, quantum mechanical phase information is lost before the magnetization can tunnel back and forth several times.[7] For observation of coherent quantum tunneling of the magnetization to be possible, the tunneling rate must be greater than the rate of decoherence in the system. Decoherence in molecular nanomagnets is caused mainly by intermolecular dipolar and exchange interactions (which can eventually cause long-range ordering),[8] and coupling to lattice vibrations (phonons) and nuclear spins.[9] Coherent quantum tunneling of the magnetization is a form of macroscopic quantum coherence. The observation of macroscopic quantum coherence is a holy grail in the study of how the quantum world of molecules transforms into the classical world that we experience. Quantum tunneling of the magnetization is made possible by the occurrence of superposition states. These superposition states are the key feature of quantum computing,[7] which is why molecular magnets that show superposition states have recently been at the center of much attention regarding quantum computing;[6,10–12] decoherence rates of 10^{+6}–10^{+7} Hz were found.

Tetranuclear nickel(II) cubane complexes have proven to be a class of complexes with highly interesting magnetic properties. Although many such complexes have been reported,[13] the magnetic properties of fewer than 20 have been investigated in detail. Of these, in most cases the superexchange interaction is predominantly ferromagnetic, leading to a high-spin ($S = 4$) ground state. In several cases the magnetic anisotropy and/or the magnetization dynamics have been investigated.[14–21] From these studies it can be concluded that the second-order axial anisotropy is usually negative, but that quantum tunneling of the magnetization is often very efficient, sometimes to the point of disappearance of any magnetic hysteresis. The actual tunneling rate has been determined for only one [Ni_4] cubane complex ($\nu_{\mathrm{tunnel}} = 0.2\ s^{-1}$ at 40 mK for [{Ni(hmp)(dmb)(Cl)}$_4$] (Hhmp = 2-hydroxymethylpyridine; dmb = 3,3′-dimethyl-1-butanol), which is also the highest reported rate for ground-state tunneling).[8] This is much slower than the rate of decoherence; the tunneling will therefore be incoherent. This tunneling of the magnetization persists in complexes that have fourfold symmetry, in which second-order transverse anisotropy is absent. In that case, tunneling is a result of an effective fourth-order transverse anisotropy, which has its origin in the quantum mixing between the ground spin multiplet and excited multiplets by the single-ion anisotropy[22] or by the antisymmetric exchange interactions.[23,24] A decrease in the cluster symmetry allows second-order transverse ZFS, which can increase the QTM rate further, as shown for Mn_4 complexes.[25,26]

Here, we present the synthesis and experimental study of a nickel(II) cubane complex of extremely low (C_1) symmetry, which cannot be increased by idealization of its structure. The complex was studied by magnetic resonance methods, specific heat measurements, and fast AC susceptibility investigations. Of particular interest is the complete absence of slow relaxation of the magnetization, down to 23 mK, giving a huge value for the lower limit of the QTM rate, $\Gamma_{\mathrm{tunnel}} = 5.8 \times 10^5\ s^{-1}$, which is of the order of the expected decoherence rate, making this complex a prime candidate for the observation of coherent tunneling of the magnetization.

Experimental Section

Synthesis: All syntheses were performed under aerobic conditions using commercial reagents without further purification. The H_2phpz ligand was prepared according to reported procedures.[27]

[Ni_4(OH)(OMe)$_3$(Hphpz)$_4$(MeOH)$_3$](MeOH) (1): A solution of H_2phpz (161 mg, 0.9 mmol) and Bu_4NOH (2 mmol, added as commercial 0.1 M methanolic solution (2 mL) in methanol (10 mL) was added dropwise to a solution of [$Ni(ClO_4)_2$]·6H_2O (365 mg, 1 mmol) in methanol (10 mL) over a period of 1 min. A pale green microcrystalline precipitate formed overnight (213 mg, 73%). Repeated analyses demonstrated that the product rapidly exchanged MeOH solvate molecules for H_2O molecules. IR: $\tilde{\nu}$ = 2925.8 (m), 2815.7 (m), 1598.4 (s), 1558.1 (m), 1460.6 (s), 1305.7 (s), 1266.9 (m), 1254.3 (m), 1122.6 (w), 1040.5 (s), 848.2 (s), 789.8 (w), 753.5 (s), 641.6 (w), 575.7 (w), 454.8 cm^{-1} (m); elemental analysis calcd

(%) for **1**·5 H_2O(−MeOH): C 45.15; H 5.60; N 9.16; found: C 44.81; H 4.80; N 9.66.

Crystallography: Data for complex **1** were collected at 150 K by using a Bruker APEX II CCD diffractometer on station 9.8 of the Synchrotron Radiation Source at CCLRC Daresbury Laboratory, 0.6894 Å, from a silicon (111) monochromator. The structure was solved by direct methods and refined using the SHELXTL suite of programs. All non-hydrogen atoms were refined anisotropically except for those sites not fully occupied. Displacement and geometrical restraints were used in modeling the partially occupied molecules. If possible, the hydrogen atoms were placed geometrically. Most methyl and hydroxyl hydrogen atoms were found in the difference map. If they could not be found, they were omitted from the refinement. The hydrogen atoms were refined using a riding model for C−H bonds. For the O−H bonds the distance was restrained and the displacement parameter ridden on the oxygen.

Magnetic measurements: Magnetic susceptibility (both DC and AC) and magnetization measurements down to 1.8 K were performed with a Quantum Design MPMS XL5 SQUID magnetometer. Corrections for diamagnetic contributions of the sample holder to the measured magnetization and of the sample to the magnetic susceptibility were performed experimentally and by using Pascal's constants, respectively.

High-frequency and high-field electron paramagnetic resonance (HFEPR): Measurements were performed at Stuttgart and at the National High Magnetic Field Laboratory (NHMFL). A single-pass transmission-type spectrometer in which the sub-terahertz waves propagate in cylindrical light pipes, as described previously, was used in the HFEPR experiments at the NHMFL.[28] Sub-terahertz frequencies were generated by Gunn oscillators, operating at either 95 ± 3 or 110 ± 3 GHz, respectively. Higher frequencies were obtained using Schottky diode-based multipliers. An Oxford Instruments 15/17 T superconducting magnet was used. Experiments were performed on a pellet pressed from the neat material mixed with KBr. The typical sample weight was 100 mg.

Measurements at Stuttgart were performed on a quasi-optical spectrometer that uses backward-wave oscillators as tunable radiation sources, and an Oxford Instruments Spectromag 4000 8 T optical split coil magnet.[29] The spectrometer was converted for field-swept measurements by changes in the software only.

The spectra were simulated using two different programs: a home-developed program Spin by A. Ozarowski, and Easy-Spin by S. Stoll.[30]

Specific heat: The specific heat of a powdered microcrystalline sample was measured using a Quantum Design PPMS. The sample was mixed with Apiezon N grease to increase the thermal contact with the calorimeter and the homogeneity in temperature across the sample. The relaxation method was used in which the temperature of the calorimeter block was monitored over time after switching pulses of heat power on and off.[31,32] The pulses were calibrated to give maximum temperature steps of about 2% of the absolute temperature. The contributions arising from the empty calorimeter and the grease were measured separately, and subtracted from the data to obtain the heat capacity of the sample.

AC susceptibility experiments: The AC susceptibility was measured using a combination of two different setups. In the first a home-made mutual inductance susceptometer was thermally anchored to the mixing chamber of a ^{3}He–^{4}He dilution refrigerator, which enabled measurements to be performed from 0.09 K up to 3.5 K in the frequency range $333\ \text{Hz} < \nu_{AC} < 13\ \text{kHz}$. A powdered sample was fixed inside the secondary coil of the susceptometer by mixing it with Apiezon N grease. To attain even lower temperatures and higher frequencies, we made use of a second home-made system in which the sample and susceptometer were installed inside the plastic mixing chamber of an especially designed ^{3}He–^{4}He dilution refrigerator, therefore ensuring perfect thermal contact with the ^{3}He–^{4}He mixture and enabling experiments down to the base temperature of about 23 mK. To avoid any contamination of the mixture, the powdered sample of **1** was embedded in Araldite. We checked that this sample showed the same magnetic behavior above 1.8 K as the original powder, both before the ultralow-temperature experiments and afterward, indicating that the complex remained intact. The susceptometers consisted of two oppositely wound pickup coils and a superconducting excitation coil. The two setups used a lock-in amplifier to detect the voltages arising from in-phase and out-of-phase magnetic signals. Unfortunately, the out-of-phase signals measured in the high-frequency susceptometer were below its sensitivity limits. Therefore, we report χ'' data for frequencies up to only 13 kHz. These low-temperature data were calibrated against susceptibility measurements performed with a Quantum Design MPMS® XL 5 SQUID magnetometer in the temperature region of overlap between the two setups.

Other physical measurements: IR spectra were recorded as KBr pellet samples on a Nicolet 5700 FTIR spectrometer. Elemental analyses were performed in-house on a Perkin–Elmer Series II CHNS/O Analyzer 2400, at the Servei de Microanàlisi of CSIC, Barcelona, Spain.

Results

Synthesis: The reaction of $[Ni(ClO_4)_2]$ and H_2phpz in methanol in the presence of the base Bu_4NOH resulted in the immediate formation of a microcrystalline precipitate. The dropwise addition of the deprotonated ligand to the Ni^{II} solution avoided an excess of $Hphpz^-$ (H_2phpz = 3-methyl-5-(2-hydroxyphenyl)pyrazole) in the system, thus preventing the precipitation of the known monomeric adduct $[Ni(Hphpz)_2]$,[33] which was otherwise found in variable amounts in the crude product. The identity of the product as crystallized from the reaction mixture was established by synchrotron single-crystal X-ray crystallography to be $[Ni_4(OH)(OMe)_3(Hphpz)_4(MeOH)_3](MeOH)$ (**1**), formed according to Equation (2).

$$4\,[Ni(ClO_4)_2] + 4\,H_2phpz + 8\,Bu_4NOH + 7\,MeOH \rightarrow [Ni_4(OH)(OMe)_3(Hphpz)_4(MeOH)_3](MeOH) + 8\,Bu_4N(ClO_4) + 7\,H_2O \quad (2)$$

Layering of chloroform or dichloromethane solutions of this product with diethyl ether or hexane resulted in formation of diamagnetic $[Ni(Hphpz)_2]$. This underscores the lability of complex **1** in solvents other than MeOH, which opens a facile route to the other thermodynamically stable product observed in this reaction system, namely the monomeric species. The ability of H_2phpz to induce the aggregation of metal ions into molecular clusters had already been shown by the formation of octanuclear and trinuclear Mn^{III} complexes.[33,34] The present results confirm that ability.

Crystal structure: Table 1 summarizes the crystallographic details of **1**, while selected structural parameters are given in the Supporting Information, Table S1. Complex **1** consists of a tetranuclear nickel(II) aggregate (Figure 1 and Supporting Information, Figure S1) with a pseudo-cubane $[Ni_4O_4]$ core composed of one pentacoordinated and three hexacoordinated Ni^{II} ions, and triply bridging oxygen atoms from one hydroxide and three methoxide ligands. For each metal ion, the octahedral coordination sphere (Ni1, Ni3, Ni4) is completed by one chelating pyrazolyl/phenoxide ligand $Hphpz^-$ and one terminal MeOH molecule. The pentacoordinated Ni^{II} center (Ni2) lacks the MeOH ligand and shows a distorted geometry, between square pyramidal and trigonal bipyramidal ($\tau = 0.33$).[35] Of the four chelating ligands,

Table 1. Crystallographic data for $[Ni_4(OH)(OMe)_3(Hphpz)_4(MeOH)_3]$-(MeOH) (**1**).

crystal shape/color	lath/green
crystal size [mm^3]	$0.30\times0.06\times0.02$
formula	$C_{47.75}H_{65}N_8Ni_4O_{12.75}$
formula wt [$g\,mol^{-1}$]	1189.92
crystal system	monoclinic
space group	$P2_1/c$
a [Å]	19.1695(15)
b [Å]	20.6612(16)
c [Å]	13.5460(11)
α [°]	90
β [°]	92.820(2)
γ [°]	90
V [$Å^3$]	5358.6(7)
Z	4
T [K]	150(2)
ρ_{calc} [$g\,cm^{-3}$]	1.475
wavelength (synchrotron) [Å]	0.6894
μ [mm^{-1}]	1.451
unique data	16184
R,[a] $wR2$[b] ($I>2\sigma(I)$)	0.0497, 0.1376 (11863 reflns)

[a] $R=\Sigma\,|F_o|-|F_c|\,|\,\Sigma\,|F_o|$. [b] $wR2=[\Sigma[w(F_o^2-F_c^2)^2]/\Sigma[w(F_o^2)^2]]^{1/2}$.

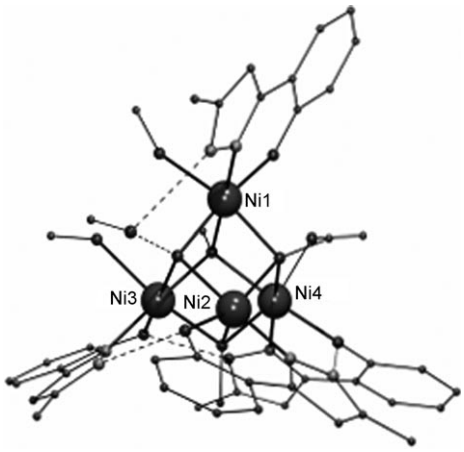

Figure 1. Representation of the molecular structure of **1**, in which only Ni atoms are labeled. Hydrogen atoms are not shown, and broken lines indicate hydrogen bonding interactions.

which are essentially flat, three form a kind of "crown" around the cluster, each ligand forming an N–H···O hydrogen bond with the adjacent ligand. An idealized C_3 cluster symmetry is disrupted by the presence of the five-coordinate Ni^{II} center, the μ_3-OH^- ligand of the core, and the coordination sphere around Ni1. Thus, the pseudo-cubane cluster **1** has no idealized symmetry at all, which renders it a very rare example within the family of $[Ni_4O_4]$ cubanes (see below). The structure of **1** also shows a solvate MeOH molecule interacting directly with the core of the cluster through an O-H···O hydrogen bond (Figure 1).

The unexpected low symmetry of **1** led us to consider the symmetries of reported $[Ni_4]$ cubanes. In a recently reported survey of $[Ni_4O_4]$ cubanes, the idealized symmetry and the deviation from that symmetry were considered on the basis of Ni–O bond lengths and angles only.[13] However, the nature of the ligand carrying the oxygen atom has also been shown to influence magnetic properties strongly,[36] and the same is true for the nature of the remaining ligands.[37,38] In addition, the nature and symmetry of the arrangement of all the ligands around the metal centers will determine the possible presence and magnitude of the different ZFS parameters. Therefore we have reexamined the structure of the 51 complexes with the $[Ni_4O_4]$ core deposited at the Cambridge Structure Database (version 5.28, May 2007), and have classified them into six groups, depending on their idealized symmetry, taking into consideration the immediate ligand environment of the metal centers and the connectivity between them which determines the number of different exchange coupling constants that can occur (Supporting Information, Figure S2). Surprisingly, this survey shows that **1** is one of the few $[Ni_4O_4]$ cubanes with no (idealized) symmetry elements at all; only three other examples are known.[39,40]

Magnetic susceptibility: The variable-temperature bulk magnetization properties of **1** were studied by SQUID magnetometry in the 1.8–300 K range in an applied magnetic field of 0.5 T (Figure 2). At 300 K the $\chi_M T$ product is

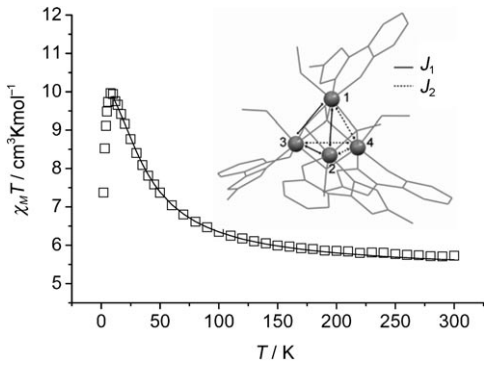

Figure 2. The measured $\chi_M T$ product as a function of T at an applied field of 0.5 T (□), and the fit using the parameters described in the text (——). The inset shows the spin coupling scheme for this fit.

5.72 $cm^3\,K\,mol^{-1}$, which is slightly above the expected value of four noncoupled Ni^{II} ions with commonly found $g=2.25$[41] (5.07 $cm^3\,K\,mol^{-1}$). This increases on cooling until a maximum of 9.96 $cm^3\,K\,mol^{-1}$ is reached at 8 K, after which it decreases abruptly at lower temperatures, down to 7.37 $cm^3\,K\,mol^{-1}$ at 1.8 K. These results suggest the presence of predominantly ferromagnetic intramolecular interactions leading to an $S=4$ ground state, although the $\chi_M T$ value for this state (12.66 $cm^3\,K\,mol^{-1}$ for $g=2.25$) is never reached. This low maximum value and the decrease observed at lower temperatures are attributed to ZFS, saturation effects, and the possible mixing, induced by the applied field, of the $S=4$ multiplet with excited multiplets. This is supported by AC susceptibility data measured at zero field. These experiments give a $\chi_M T$ peak of about 11.6 $cm^3\,K\,mol^{-1}$, which is much closer to the value expected for an $S=4$ ground state,

and a three times smaller decrease at 2 K. An estimate of the exchange coupling constants, and therefore of the magnetic energy level scheme, of complex **1** was obtained by modeling the higher-temperature ($T>10$ K) experimental data, using full diagonalization procedures implemented in the program CLUMAG.[42] Despite the C_1 symmetry of the complex, which allows six distinct exchange interactions, an approximation was sought by employing the minimum number of J values, to avoid overparametrization. The use of a single J value produced no satisfactory simulation, but a good fit (Figure 3) was obtained with a two-J model, described by the spin Hamiltonian given by Equation (3), constructed according to the numbering scheme of Figure 1.

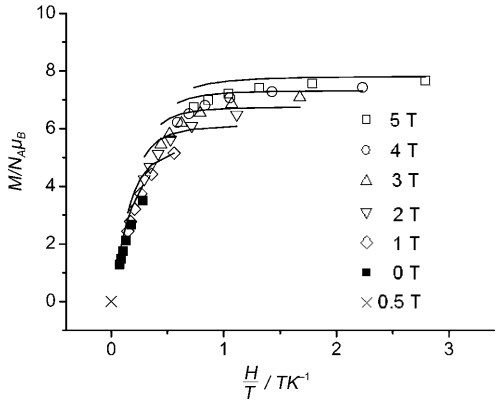

Figure 3. Isofield reduced magnetization as a function of H/T plots for **1**, collected at different constant magnetic fields (various symbols, defined on the figure) and fits as described in the text (solid lines).

$$\mathscr{H}^{ex} = -J_1(\hat{\mathbf{S}}_1\cdot\hat{\mathbf{S}}_2 + \hat{\mathbf{S}}_1\cdot\hat{\mathbf{S}}_3 + \hat{\mathbf{S}}_2\cdot\hat{\mathbf{S}}_3) - J_2(\hat{\mathbf{S}}_1\cdot\hat{\mathbf{S}}_4 + \hat{\mathbf{S}}_2\cdot\hat{\mathbf{S}}_4 + \hat{\mathbf{S}}_3\cdot\hat{\mathbf{S}}_4) \quad (3)$$

Here, the different Ni···Ni pathways for magnetic exchange were divided into two groups: those within Ni_2 pairs bridged by one μ-OH^- group and one μ-OMe^- ligand (J_1), and those involving two μ-OMe^- bridges. The calculation provided the parameters $J_1=+13.0$ cm^{-1}, $J_2=+0.5$ cm^{-1} and $g=2.29$, with an error of $R^2=4.6\times10^5$ ($R^2=\Sigma(\chi_M T_{calc}-\chi_M T_{obs})^2/\Sigma(\chi_M T_{obs})^2$). These results are in agreement with reported magnetostructural correlations which predict ferromagnetic interactions between Ni^{II} ions exhibiting Ni–O–Ni angles smaller than 99°.[40] In complex **1**, only one angle (99.34°) is larger than this limit. The ferromagnetic exchange interactions lead to an $S=4$ spin ground state with first excited states $S=3$ and $S=2$ lying at only 1.84 and 3.22 cm^{-1} higher energies, respectively. Because of these small energy separations, extensive mixing between the spin states can be expected.

Variable-temperature isofield reduced magnetization data were collected at various magnetic fields (0.5, 1, 2, 3, 4, and 5 T) to characterize the spin ground state. The isofield lines are not superposable (Figure 3), indicating the presence of ZFS of the ground state. These data were simulated through a full diagonalization procedure by using the spin Hamiltonian in Equation (1) for the $S=4$ ground state. The fit (Figure 3) produced the parameters $D=-1.11$ cm^{-1}, $E=0.02$ cm^{-1} and $g=2.33$. Using a positive D value led to a considerably worse fit, and gave $D=1.01$ cm^{-1}, $E=0.11$ cm^{-1}, and $g=2.30$. The discrepancy between the experimental and calculated points is because the $S=4$ ground state is not well isolated from the excited states, which leads to both mixing between spin states (see below) and thermal occupation of excited spin states. Thus, the calculated ZFS and g value parameters should be taken as only approximate. Much more reliable parameter values can be obtained from HFEPR measurements, which we therefore carried out.

HFEPR measurements: Typical HFEPR spectra recorded on powder samples of **1** in the high-frequency region (≈270–370 GHz) showed two very broad transitions (Figure 4) that were interpreted as the parallel and perpendicular turning points of the transition between the $M_S=\pm4$ and $M_S=\pm3$ levels of the $S=4$ spin manifold. Lower-frequency spectra had additional fine structure (Figure 4) superposed on the broad resonances. The spectra were simu-

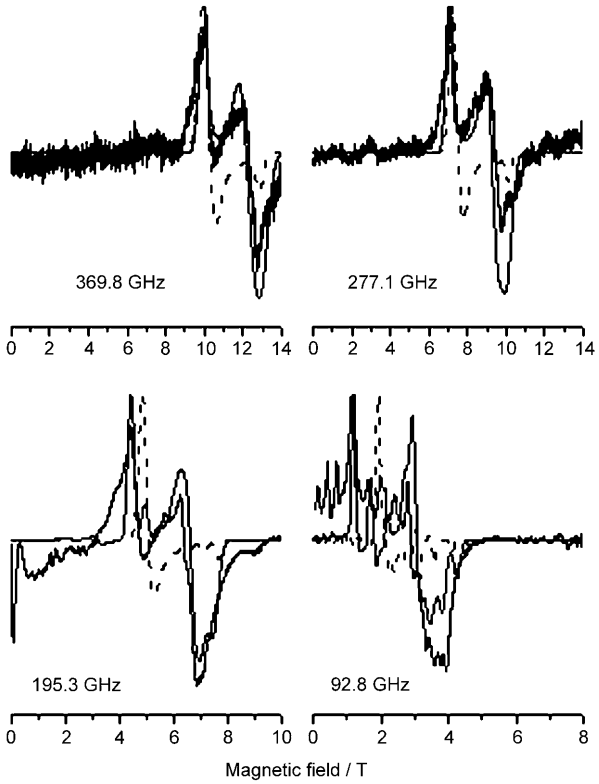

Figure 4. HFEPR spectra of **1** at $T=5.0$ K at $\nu=369.8$, 277.1, 195.3, and 92.76 GHz, as indicated on the figure. Solid traces are experiments; thick black traces are simulations with $D<0$ ($D=-0.263$ cm^{-1}, $E=0.04$ cm^{-1}, $g_{iso}=2.25$); broken traces are simulations with $D>0$ ($D=+0.30$ cm^{-1}, $E=0.04$ cm^{-1}, $g_{iso}=2.4$). The g strain parameters $\Delta g_\perp=0.15$ and $\Delta_\parallel=0.10$, as well as field-independent linewidths $\Delta H_\perp=1000$ G and $\Delta H_\parallel=667$ G were employed.

lated using the second-order ZFS spin Hamiltonian [Eq. (4)] acting on the $S=4$ spin ground multiplet. The best agreement between the simulations and experiment was obtained for the axial ZFS parameter $D=-0.263\pm0.003\ cm^{-1}$, and $E=0.04\pm0.01\ cm^{-1}$, which therefore give a theoretical anisotropy energy barrier $U=4.21$ (5) cm^{-1}. Importantly no reasonable fit was obtained for positive values of D (Figure 4). The fits are relatively insensitive to the E parameter, because of the large linewidth, especially at high frequencies. Extensive simulations showed that the best fit is obtained assuming a constant linewidth of 1000 G for perpendicular turning points and 667 G for parallel turning points in addition to a sizable distribution of g parameters (g strain) of $\Delta g_{\perp}=0.15$ and $\Delta g_{\parallel}=0.10$, which accounts for the observed line broadening with increasing frequency/field. This g strain is much larger than that found for other molecular magnets, for example, $Mn_{12}Ac$.[43,44] The isotropic g value is 2.25, which is typical for both single-ion Ni^{II} complexes and their clusters.[41]

$$\mathscr{H}=\beta\mathbf{B}\cdot\mathbf{g}\cdot\hat{\mathbf{S}}+D(\hat{S}_z{}^2-S(S+1)/3)+E(\hat{S}_x{}^2-\hat{S}_y{}^2) \qquad (4)$$

A survey of reported ZFS parameters for $[Ni_4]$ cubane clusters (Table 2) shows that the D value of **1** is among the lowest values reported for such clusters. The structure that is visible in the lowest-frequency spectrum (93 GHz) shows that many different transitions become allowed at low fields, because ZFS and Zeeman terms are of comparable magnitude. This leads to extensive mixing between M_S levels and significant magnetic resonance intensity of nominally forbidden EPR transitions. Not all features in the experimental spectrum are reproduced in the simulation. This raises the possibility that we were observing an excited spin state ($S=3$). However, a temperature-dependent experiment performed at 93 GHz was inconclusive: although some temperature-dependent spectral changes were indeed observed, there was no clear thermal activation of particular spectral features that would allow us to attribute them to an $S=3$ spin state. Another explanation is that the additional features are a result of mixing between the ground spin state and the low-lying $S=3$ state which will allow intermultiplet transitions, as was recently observed.[45] In summary, we advance the following explanation: at high frequencies and fields, the $M_S=4$ state of the $S=4$ multiplet is stabilized with respect to the other states, and a relatively simple spectrum is observed. At low frequencies and fields, the multiplets are extensively mixed, rendering an analysis of the EPR spectra in terms of separated multiplets impossible. Attempted fits in the full Hilbert space of the molecule are doomed to fail because of the large number of free parameters allowed by the low symmetry of **1**.

Specific heat: The measurement of the specific heat provides information on the ZFS, the process of relaxation toward thermal equilibrium, and the occurrence of long-range magnetic ordering.[32] Above $T=3$–4 K, the molar specific heat of a sample of **1** (Figure 5) is dominated by the contribution of vibration modes. This contribution can be fitted reasonably well up to room temperature by the sum of three contributions: a Debye term, accounting for the specific heat of acoustic phonon modes, plus two Einstein terms that simulate the specific heat owed to intramolecular vibrations (optical modes). This constitutes the simplest possible approximation to describe the complex vibrational spectrum of this molecule. Therefore, the Debye temperature $\theta_D\approx25$ K that ensued from these data must be taken as an estimate. In any case, this value is of the same order of magnitude as those found for other crystals of molecular clusters.[26,32,46] Below $T=3$ K, additional contributions to the specific heat appear. These are associated with the magnetic degrees of freedom of the molecules. The shape of the experimental curve suggests the presence of a Schottky anomaly, with a peak centered near 1.5 K. This anomaly is associated with the ZFS of the magnetic levels as represented by the anisotropy terms of the spin Hamiltonian. We have calculated this contribution using the simplest spin Hamiltonian [Eq. (1)] for the $S=4$ ground state multiplet and taking $D=-0.26\ cm^{-1}$ as found by HFEPR. The results calculated for $E=0$ lie clearly above the measured values, whereas a better agreement is obtained for $E=-D/3$. A nonzero E value reflects additional splittings in the low-lying spin levels that are not a result of uniaxial anisotropy. Other mechanisms for inducing additional level splittings include effects owed to mixing between spin states, which can be expected given

Table 2. Reported ZFS parameters for ferromagnetic $[Ni_4]$ cubane complexes.

Complex	ZFS parameters [cm^{-1}]	Method	Ref.
$[Ni_4(OH)(OMe)_3(Hphpz)_4(MeOH)_3]$[a]	$D=-0.263$, $E=0.04$	HFEPR	this work
$[Ni_4(thme)_4(MeCN)_4]$[b]	$D=-0.43$, $E=0.0172$	χ	[14]
$[Ni_4(sae)_4(MeOH)_4]$[c]	$D=-0.93$, $B_4{}^0=-0.00043$, $\lvert E\rvert=0.023$, $B_4{}^4=-0.0021$	INS, FDMRS[d]	[17]
$[Ni_4(sae)_4(MeOH)_4]$[c]	$D=-1.01$	M vs. H	[17]
$[Ni_4(hmp)_4(dmb)_4(Cl)_4]$[e]	$D=-0.60$, $B_4{}^0=-0.00012$, $B_4{}^4=0.0004$[f]	HFEPR	[18,19]
$[Ni_4(hmp)_4(MeOH)_4(Cl)_4]$[e]	$D=-0.715$, $B_4{}^0=-0.00017$[f]	HFEPR	[18]
$[Ni_4(hmp)_4(MeOH)_4(Br)_4]$[e]	$D=-0.632$, $B_4{}^0=-0.00015$[f]	HFEPR	[18]
$[Ni_4(hmp)_4(EtOH)_4(Cl)_4]$[e]	$D=-0.610$, $B_4{}^0=-0.00012$[f]	HFEPR	[18]
$[Ni_4(pym)_4(CH_3OH)_4(Cl)_4]$[g]	$D=-0.47$	χ	[20]
$[Ni_4(pym)_4(CH_3OH)_4(N_3)_4]$[g]	$D=-0.10$	χ	[20]
$[Ni_4(OMe)_4(O_2CCMe_3)_4(MeOH)_4]$	$D=-0.28$	INS	[16]
$[Ni_4(OH)_4(dpa)_4]^{4+}$[h]	$D=-2.0$	χ	[21]
$[Ni_4(OAc)_4(ampdH)_4]$[i]	$D=-0.33$	χ	[15]

[a] H_2phpz = 3-methyl-5-(2-hydroxyphenyl)pyrazole. [b] thme = trihydroxymethylethane. [c] H_2sae = salicylidene-2-ethanolamine. [d] INS = inelastic neutron scattering, FDMRS = frequency domain magnetic resonance spectroscopy. [e] Hhmp = 2-hydroxymethylpyridine, dmb = 3,3′-dimethyl-1-butanol. [f] The spin Hamiltonian parameters are given for the highest ZFS species only. [g] Hpym = pyridine-2-methoxide. [h] dpa = 2,20-dipicolylamine. [i] $ampdH_2$ = 2-amino-2-methyl-1,3-propanediol

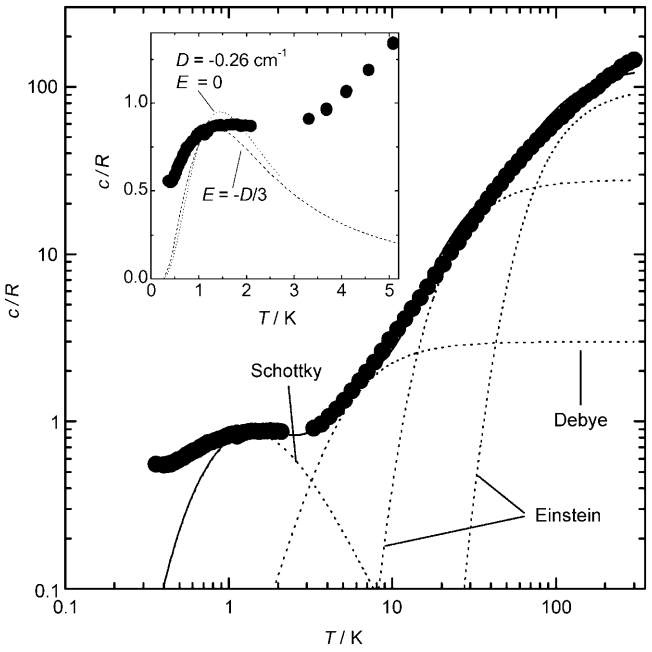

Figure 5. Specific heat measurements on **1**, showing experimental data (○), and the fit (——) with the calculated ZFS (-----), and lattice (•••••) contributions. The inset shows an expanded view of the low-temperature region. Fits obtained for two E values are displayed.

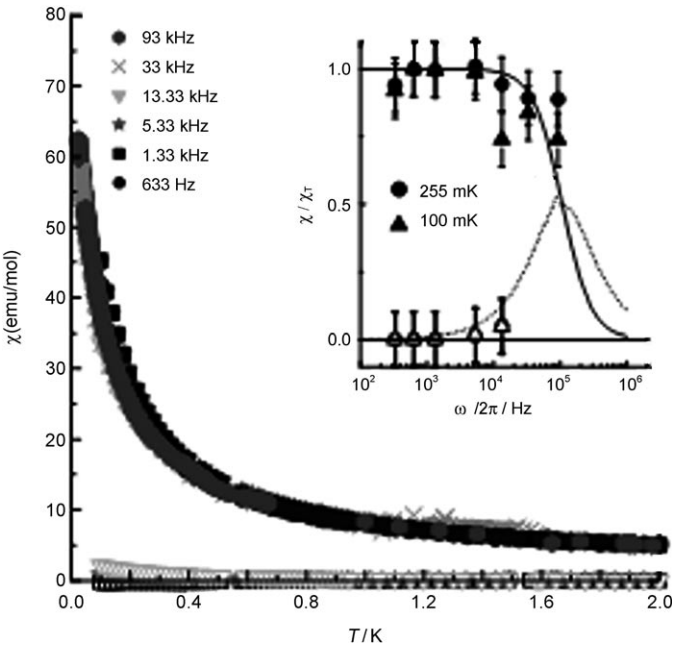

Figure 6. AC susceptibility of **1** measured at different frequencies as indicated in the figure. The inset shows the variation with frequency of χ' (filled symbols) and χ'' (open symbols) at two temperatures. Solid (χ') and dotted (χ'') lines are calculated with the Debye equations (5) and (6) using $\chi_\infty = 0$ and $\Gamma = 0.667$ MHz.

the sizable anisotropy and the small energy gap to excited spin multiplets. The optimum E parameter obtained from the simulation of the specific heat data should therefore be taken as a strong indication of the presence of interactions beyond second-order axial ZFS, rather than being considered quantitatively accurate. Therefore, we believe the specific heat results agree with those from HFEPR. Further contributions to the specific heat are observed below 0.6 K, reflecting the existence of low-lying energy states (for example, nuclear spin states) or small splittings caused by intermolecular magnetic–dipole interactions. Because the former is not expected to exceed 0.04 R mol^{-1}, we assume the latter is the case.

AC susceptibility: In spite of the Ising-like anisotropy of **1**, AC susceptibility measurements down to 1.8 K show no signature of slow magnetization dynamics. Therefore we embarked on ultralow-temperature studies of the magnetization dynamics. The frequency-dependent susceptibility of **1** measured down to 23 mK at frequencies up to 92 kHz show typical (super)paramagnetic behavior (Figure 6). It is reassuring that data measured on two samples using two different setups overlap very well in their common temperature ranges. For temperatures above 300 mK the susceptibility is independent of frequency ν_{AC}. Below this temperature, a very small decrease in χ' with increasing ν_{AC} was observed (see the data on the Figure 6 inset) accompanied by the onset of a weak imaginary component χ''. Yet the difference between the curves measured at 33 kHz and 91.55 kHz is only 7% at 23 mK. Despite possessing a sizable anisotropy energy barrier ($U \approx 4.21$ cm^{-1}) compared with the experimental temperature, Ni_4 clusters show therefore no clear signature of the superparamagnetic blocking, or SMM behavior, that is characteristic of other molecular nanomagnets such as Mn_{12}, Fe_8, or Mn_4.[2] The susceptibility data show instead that the spin reversal remains extremely fast even in the neighborhood of the absolute zero of temperature. To obtain a lower limit for the magnetic relaxation rate Γ, we note that, for weakly interacting spins, the susceptibility is expected to follow Debye's law [Eqs. (5) and (6)], in which χ_{eq} and χ_∞ are the equilibrium and high-frequency (adiabatic) limits of the susceptibility, respectively, and $\omega = 2\pi\nu_{AC}$ is the angular frequency corresponding to the oscillation frequency used in the AC susceptibility measurement. The weak dependence of χ' on ω and the very small values of χ'' indicate therefore that Γ is much larger than the highest AC frequency employed, $\omega_{max} = 5.8 \times 10^5$ rad s^{-1}.

$$\chi' = \chi_\infty + \frac{\chi_{eq} - \chi_\infty}{1 + (\omega/\Gamma)^2} \quad (5)$$

$$\chi'' = \frac{(\chi_{eq} - \chi_\infty)}{1 + (\omega/\Gamma)^2}(\omega/\Gamma) \quad (6)$$

This is illustrated in the Figure 6 inset, in which the solid lines show χ' and χ'' calculated using Equations (5) and (6) (with $\chi_\infty = 0$, for simplicity) for $\Gamma = 0.667$ MHz. The same data show also that Γ depends only weakly (that is, not exponentially) on temperature.

The relaxation mechanism must therefore involve direct tunneling between the two lowest-lying states, with $M_s = \pm 4$. This is not unexpected, since the population of excited magnetic energy levels can be safely neglected below 100 mK. However, as we argue next, conventional spin–lattice relaxation mechanisms do not seem to account for the very large rates estimated from the experiments. At millikelvin temperatures, the only spin–phonon process that is expected to contribute to tunneling relaxation is the direct one.[47,48] Two-phonon processes such as Raman and Orbach processes are expected to be negligible because of the absence of phonons at these low temperatures.[47] Furthermore, they always give rise to a strong dependence of Γ on temperature, which is not observed experimentally. The probability of a direct phonon-induced tunneling transition between the tunnel-split $M_S = \pm 4$ states can be estimated by Fermi's golden rule [Eq. (7)], in which q is a constant depending on the strength of the spin–phonon interaction, ΔE is the energy splitting of the ground-state doublet, and $|V_{m=\pm 4}|$ is the matrix element of the spin–phonon interaction for the tunnel-split $M_S = \pm 4$ states.[48–52] The latter depends on the exact wavefunctions, and thus also on the different terms contributing to the spin Hamiltonian. In particular, it depends on the competing effects between terms of the Hamiltonian that induce tunneling (for example, transverse ZFS and transverse dipolar and hyperfine fields) and those that tend to block it (for example, bias magnetic fields induced by dipolar interactions). It is therefore difficult to estimate it accurately. Our preliminary calculations suggest nevertheless that $\Gamma_{m=\pm 4} < 10^{-6}\ s^{-1}$, that is, remarkably, almost 12 orders of magnitude smaller than the lower limit found for the spin–lattice relaxation rate of **1**.

$$\Gamma_{m=\pm 4} \approx q(\Delta E)^3 |V_{m=\pm 4}|^2 \qquad (7)$$

Clearly, another tunneling mechanism must dominate relaxation to equilibrium at very low temperatures.[26,48,53] For a deeper insight into the physical nature of this mechanism, susceptibility data extending to higher frequencies, in the megahertz range, would be highly desirable, thus enabling a direct determination of Γ as a function of temperature and magnetic fields. These experiments are under way.

Conclusion

We have presented a comprehensive study of a novel ferromagnetically coupled [Ni_4] cubane. We have shown that its low symmetry leads to extraordinarily fast magnetization relaxation down to the lowest temperature; this is a result of a combination of effects causing the loss of pure uniaxial anisotropy, including second-order transverse zero-field splitting and spin-mixing effects. In Ni_4 complexes, decoherence rates are expected to be small, owing to the virtual absence of metal nuclear spins and weak intermolecular dipolar interactions. For this reason, **1** might be an excellent candidate for observation of quantum coherent tunneling at zero field. Such extremely fast tunneling might occur also in other low-symmetry complexes such as some Fe_4 complexes.[54]

Acknowledgements

Financial support from the following sources is gratefully acknowledged: German Science Foundation (DFG), German Academic Exchange Service (DAAD), Project NAMESBI (Spanish Strategic Action on Nanoscience and Nanotechnology), Project MOLBIT (Spanish Ministry of Science and Education), Integrated Action between Spain and Germany (HA2006-0051), and Network of Excellence MAGMANet. NHMFL is supported by the National Science Foundation (Cooperative Agreement DMR 0654118) and the State of Florida. We thank A. Ozarowski and S. Stoll for the EPR simulation software.

[1] R. Sessoli, D. Gatteschi, A. Caneschi, M. A. Novak, *Nature* **1993**, *365*, 141.
[2] D. Gatteschi, R. Sessoli, J. Villain, *Molecular Nanomagnets*, Oxford University Press, Oxford, **2006**.
[3] L. Thomas, F. Lionti, R. Ballou, D. Gatteschi, R. Sessoli, B. Barbara, *Nature* **1996**, *383*, 145.
[4] a) J. R. Friedman, M. P. Sarachik, J. Tejada, R. Ziolo, *Phys. Rev. Lett.* **1996**, *76*, 3830; b) M. Hernandez, X. X. Zhang, F. Luis, J. Bartolome, J. Tejada, R. Ziolo, *Europhys. Lett.* **1996**, *35*, 301.
[5] W. Wernsdorfer, R. Sessoli, *Science* **1999**, *284*, 133.
[6] S. Bertaina, S. Gambarelli, T. Mitra, B. Tsukerblat, A. Müller, B. Barbara, *Nature* **2008**, *453*, 203.
[7] E. del Barco, A. D. Kent, E. C. Yang, D. N. Hendrickson, *Phys. Rev. Lett.* **2004**, *93*, 157202.
[8] E. C. Yang, W. Wernsdorfer, L. N. Zakharov, Y. Karaki, A. Yamaguchi, R. M. Isidro, G. D. Lu, S. A. Wilson, A. L. Rheingold, H. Ishimoto, D. N. Hendrickson, *Inorg. Chem.* **2006**, *45*, 529.
[9] M. Dube, P. C. E. Stamp, *Chem. Phys.* **2001**, *268*, 257.
[10] A. Ardavan, O. Rival, J. J. L. Morton, S. J. Blundell, A. M. Tyryshkin, G. A. Timco, R. E. P. Winpenny, *Phys. Rev. Lett.* **2007**, *98*, 057201.
[11] G. Mitrikas, Y. Sanakis, C. P. Raptopoulou, G. Kordas, G. Papavassiliou, *Phys. Chem. Chem. Phys.* **2008**, *10*, 743.
[12] C. Schlegel, J. van Slageren, M. Manoli, E. K. Brechin, M. Dressel, *Phys. Rev. Lett.* **2008**, *101*, 147203.
[13] K. Isele, F. Gigon, A. F. Williams, G. Bernardinelli, P. Franz, S. Decurtins, *Dalton Trans.* **2007**, 332.
[14] M. Moragues-Cánovas, M. Helliwell, L. Ricard, E. Rivière, W. Wernsdorfer, E. Brechin, T. Mallah, *Eur. J. Inorg. Chem.* **2004**, 2219.
[15] K. G. Alley, R. Bircher, H. U. Güdel, B. Moubaraki, K. S. Murray, B. F. Abrahams, C. Boskovic, *Polyhedron* **2007**, *26*, 369.
[16] G. Chaboussant, R. Basler, H. U. Güdel, S. Ochsenbein, A. Parkin, S. Parsons, G. Rajaraman, A. Sieber, A. A. Smith, G. A. Timco, R. E. P. Winpenny, *Dalton Trans.* **2004**, 2758.
[17] A. Sieber, C. Boskovic, R. Bircher, O. Waldmann, S. T. Ochsenbein, G. Chaboussant, H. U. Güdel, N. Kirchner, J. van Slageren, W. Wernsdorfer, A. Neels, H. Stoeckli-Evans, S. Janssen, F. Juranyi, H. Mutka, *Inorg. Chem.* **2005**, *44*, 4315.
[18] J. Lawrence, E.-C. Yang, R. Edwards, M. M. Olmstead, C. Ramsey, N. S. Dalal, P. K. Gantzel, S. Hill, D. N. Hendrickson, *Inorg. Chem.* **2008**, *47*, 1965.
[19] C. Kirman, J. Lawrence, S. Hill, E. C. Yang, D. N. Hendrickson, *J. Appl. Phys.* **2005**, *97*, 10M501.
[20] A. Escuer, M. Font-Bardia, S. B. Kumar, X. Solans, R. Vicente, *Polyhedron* **1999**, *18*, 909.
[21] J. P. Wikstrom, A. Y. Nazarenko, W. M. Reiff, E. V. Rybak-Akimova, *Inorg. Chim. Acta* **2007**, *360*, 3733.
[22] A. Wilson, J. Lawrence, E. C. Yang, M. Nakano, D. N. Hendrickson, S. Hill, *Phys. Rev. B* **2006**, *74*, 140403(R).
[23] N. Kirchner, PhD thesis, Universität Stuttgart, Stuttgart, **2006**.

[24] N. Kirchner, J. van Slageren, B. Tsukerblat, O. Waldmann, M. Dressel, *Phys. Rev. B* **2008**, *78*, 094426.
[25] N. Aliaga-Alcalde, R. S. Edwards, S. O. Hill, W. Wernsdorfer, K. Folting, G. Christou, *J. Am. Chem. Soc.* **2004**, *126*, 12503.
[26] M. Evangelisti, F. Luis, F. L. Mettes, N. Aliaga, G. Aromi, J. J. Alonso, G. Christou, L. J. de Jongh, *Phys. Rev. Lett.* **2004**, *93*, 117202.
[27] A. W. Addison, P. J. Burke, *J. Heterocycl. Chem.* **1981**, *18*, 803.
[28] A. K. Hassan, L. A. Pardi, J. Krzystek, A. Sienkiewicz, P. Goy, M. Rohrer, L. C. Brunel, *J. Magn. Reson.* **2000**, *142*, 300.
[29] J. van Slageren, S. Vongtragool, B. Gorshunov, A. A. Mukhin, N. Karl, J. Krzystek, J. Telser, A. Muller, C. Sangregorio, D. Gatteschi, M. Dressel, *Phys. Chem. Chem. Phys.* **2003**, *5*, 3837.
[30] S. Stoll, A. Schweiger, *J. Magn. Reson.* **2006**, *178*, 42.
[31] R. Bachmann, R. E. Schwall, H. U. Thomas, R. B. Zubeck, C. N. King, H. C. Kirsch, F. J. Disalvo, T. H. Geballe, K. N. Lee, R. E. Howard, R. L. Greene, *Rev. Sci. Instrum.* **1972**, *43*, 205.
[32] M. Evangelisti, F. Luis, L. J. de Jongh, M. Affronte, *J. Mater. Chem.* **2006**, *16*, 2534.
[33] a) M. Viciano-Chumillas, S. Tanase, G. Aromí, J. M. M. Smits, R. de Gelder, X. Solans, E. Bouwman, J. Reedijk, *Eur. J. Inorg. Chem.* **2007**, 2635; b) M. Viciano-Chumillas, S. Tanase, I. Mutikainen, U. Turpeinen, J. L. de Jongh, J. Reedijk, *Inorg. Chem.* **2008**, *47*, 5919.
[34] S. Tanase, G. Aromí, E. Bouwman, H. Kooijman, A. L. Spek, J. Reedijk, *Chem. Commun.* **2005**, 3147.
[35] A. W. Addison, T. N. Rao, J. Reedijk, J. van Rijn, G. C. Verschoor, *J. Chem. Soc. Dalton Trans.* **1984**, 1349.
[36] L. K. Thompson, S. K. Mandal, S. S. Tandon, J. N. Bridson, M. K. Park, *Inorg. Chem.* **1996**, *35*, 3117.
[37] L. Gutierrez, G. Alzuet, J. A. Real, J. Cano, J. Borras, A. Castineiras, *Eur. J. Inorg. Chem.* **2002**, 2094.
[38] A. R. Paital, T. Mitra, D. Ray, W. T. Wong, J. Ribas-Ariño, J. J. Novoa, J. Ribas, G. Aromí, *Chem. Commun.* **2005**, 5172.
[39] A. J. Blake, E. K. Brechin, A. Codron, R. O. Gould, G. M. Grant, S. Parsons, J. M. Rawson, R. E. P. Winpenny, *J. Chem. Soc. Chem. Commun.* **1995**, 1983.
[40] J. M. Clemente-Juan, B. Chansou, B. Donnadieu, J. P. Tuchagues, *Inorg. Chem.* **2000**, *39*, 5515.
[41] R. L. Carlin, *Magnetochemistry*, Springer Verlag, Berlin, **1986**.
[42] D. Gatteschi, L. Pardi, *Gazz. Chim. Italiana* **1993**, *123*, 231.
[43] K. Park, M. A. Novotny, N. S. Dalal, S. Hill, P. A. Rikvold, *Phys. Rev. B* **2002**, *66*, 144409.
[44] K. Park, M. A. Novotny, N. S. Dalal, S. Hill, P. A. Rikvold, *Phys. Rev. B* **2002**, *65*, 014426.
[45] S. Datta, O. Waldmann, A. D. Kent, V. A. Milway, L. K. Thompson, S. Hill, *Phys. Rev. B* **2007**, *76*, 052407.
[46] F. Luis, F. L. Mettes, J. Tejada, D. Gatteschi, L. J. de Jongh, *Phys. Rev. Lett.* **2000**, *85*, 4377.
[47] A. Abragam, B. Bleaney, *Electron Paramagnetic Resonance of Transition Ions*, Clarendon Press, Oxford, **1970**.
[48] F. Luis, F. Mettes, M. Evangelisti, A. Morello, L. J. de Jongh, *J. Phys. Chem. Solids* **2004**, *65*, 763.
[49] F. Hartmann-Boutron, P. Politi, J. Villain, *Int. J. Mod. Phys. B* **1996**, *10*, 2577.
[50] F. Luis, J. Bartolome, J. F. Fernandez, *Phys. Rev. B* **1998**, *57*, 505.
[51] M. N. Leuenberger, D. Loss, *Europhys. Lett.* **1999**, *46*, 692.
[52] F. L. Mettes, F. Luis, L. J. de Jongh, *Phys. Rev. B* **2001**, *6417*, art. no.
[53] M. Evangelisti, F. Luis, F. L. Mettes, R. Sessoli, L. J. de Jongh, *Phys. Rev. Lett.* **2005**, *95*, 227206.
[54] N. T. Madhu, J. K. Tang, I. J. Hewitt, R. Clerac, W. Wernsdorfer, J. van Slageren, C. E. Anson, A. K. Powell, *Polyhedron* **2005**, *24*, 2864.
[55] M. Koikawa, M. Ohba, T. Tokii, *Polyhedron* **2005**, *24*, 2257.
[56] A. K. Sah, C. P. Rao, P. K. Saarenketo, K. Rissanen, *Chem. Lett.* **2001**, 1296.
[57] G. Aromí, A. S. Batsanov, P. Christian, M. Helliwell, O. Roubeau, G. A. Timco, R. E. P. Winpenny, *Dalton Trans.* **2003**, 4466.
[58] S. Mukherjee, T. Weyhermuller, E. Bothe, K. Wieghardt, P. Chaudhuri, *Eur. J. Inorg. Chem.* **2003**, 863.
[59] G. S. Papaefstathiou, A. Escuer, F. A. Mautner, C. Raptopoulou, A. Terzis, S. P. Perlepes, R. Vicente, *Eur. J. Inorg. Chem.* **2005**, 879.
[60] T. K. Paine, E. Rentschler, T. Weyhermuller, P. Chaudhuri, *Eur. J. Inorg. Chem.* **2003**, 3167.
[61] M. L. Tong, H. K. Lee, S. L. Zheng, X. M. Chen, *Chem. Lett.* **1999**, 1087.
[62] M. L. Tong, S. L. Zheng, J. X. Shi, Y. X. Tong, H. K. Lee, X. M. Chen, *J. Chem. Soc. Dalton Trans.* **2002**, 1727.
[63] B. Aurivillius, *Acta Chem. Scand.* **1977**, *31*, 501.

Received: July 18, 2008
Published online: October 29, 2008

